Structural disorders in an amorphous HfO_2 film probed by x-ray absorption fine structure analysis

Deok-Yong Cho, Tae Joo Park, Kwang Duk Na, Jeong Hwan Kim, and Cheol Seong Hwang*
Department of Materials Science and Engineering, Inter-university Semiconductor Research Center, Seoul National University, Seoul 151-744, Republic of Korea

(Received 17 July 2008; revised manuscript received 1 September 2008; published 22 October 2008)

The local structural order of amorphous HfO_2 films (a-HfO_2) was examined using Hf L_3-edge x-ray absorption spectroscopy and fine structure analyses. The fine structure simulation successfully reproduced the spectral evolution of the crystalline-to-amorphous phase transition by reducing the characteristic radius for atomic ordering to ~3.5 Å. Detailed path-by-path analyses further showed that the vibrational displacement of oxygen atoms in a-HfO_2 films is highly anisotropic showing mainly lateral dispersion perpendicular to a Hf-O bond. This anisotropic structural disorder is responsible for enhancing the dielectric constant accompanying phonon mode softening in the a-HfO_2 film.

DOI: 10.1103/PhysRevB.78.132102 PACS number(s): 77.55.+f, 61.05.cj, 61.43.−j, 78.70.Dm

Amorphousness is a desirable property for high-k gate oxide materials in metal-oxide-semiconductor field effect transistors (MOSFETs) because it provides homogeneity in the dielectric properties irrespective of the local geometry of the gate stack.[1] A lack of grain boundaries in amorphous materials not only prevents the leakage current and fluctuations in the carrier concentration through local charge trapping[2] but also ensures the compositional stability during the fabrication process.[1,3] There has been considerable industrial interest in the amorphous high-k films (see, e.g., Refs. 2–4). However, to date, there are few methodologies for examining the fundamental physics of the amorphousness of high-k materials with high levels of disorder.

Knowledge on the *local* atomic structure is quite valuable because the microscopic properties, such as the dielectric response, the charge distribution, and the band gap, significantly depend on the local atomic distribution.[5] The amorphous phase of a representative high-k material, HfO_2, has been found to have a slightly higher dielectric constant than the most stable monoclinic ($P2_1/c$) phase.[6–8] The enhancement in the dielectric constant (ε) is largely due to the increase in lattice polarization ($\varepsilon_{\mathrm{lat}}$) with a softening of the phonon modes rather than to an increase in electronic polarization ($\varepsilon_{\mathrm{ele}}$).[7] The $\varepsilon_{\mathrm{ele}}$ invariance was confirmed experimentally by the similarity in the electronic structure of the amorphous and monoclinic phases [with seven nearest-neighbor (NN) oxygen atoms] except for the disorder-induced broadening of the features.[9,10] On the other hand, $\varepsilon_{\mathrm{lat}}$, which can be altered even by a tiny modulation in the local structure without changing the overall electronic structure, should be examined using a technique that can probe the detailed local atomistic structures. This can be accomplished by x-ray absorption fine structure (XAFS) analyses.

The generalized formula for the fine structure oscillation χ in electron-momentum (k) space can be fractionized as

$$\chi(k) = \sum_{j,l} \tilde{\chi}_{j,l}(k)\sin(2kR_j + \Phi_{j,l})e^{-2R_j/\lambda(k)}e^{-2k^2\sigma_j^2}, \qquad (1)$$

where $2R$, Φ, and σ^2 denote the path length, phase shift, and Debye-Waller disorder factor for each path j and final-state angular momentum l, respectively, and λ denotes the mean-free path for the final-state electron. The Fourier-transformed (FT) magnitude of extended x-ray absorption fine structure (EXAFS) in the *high* kinetic-energy region (>30 eV) reflects mainly single backscattering events, such as Hf↔O or Hf↔Hf′ paths, while the x-ray absorption near-edge structure (XANES), which concerns the quasi-free-electrons at relatively *low* kinetic energies (<40 eV),[11] reflects the scattering for all paths such as Hf→O→O→Hf or Hf→O→Hf′→Hf.

This Brief Report reports the results of the strict XAFS path analyses on a-HfO_2. XAFS oscillation of a path can be classified by its path type, such as Hf-O or Hf-O-O′-Hf, because the paths in the same path type and similar path-length range have the same level of phase shift so as to have a similar XAFS oscillation. Therefore, the XAFS simulations were performed path by path for all possible multiple-scattering paths shorter than a characteristic length 2ξ, which stands for the diameter of the atomistic order correlation. The multiple-scattering approach showed that (i) the local atomic distribution of the a-HfO_2 has a reduced characteristic length ($\xi \sim 3.5$ Å), (ii) the bond angle between O-Hf-O bonds shows significant scatter ($> \pm 10°$) even in the first shell, and (iii) the disorder in the O-Hf displacement is highly anisotropic as to have a lateral distribution perpendicular to the Hf-O bond direction. This suggests that additional lateral elastic vibrations of the Hf-O bonds can emerge to yield increases in Born effective charges and consequently the dielectric constant in a-HfO_2.[7]

HfO_2 films with a nominal thickness of ~10 nm were prepared by atomic layer deposition using a $Hf[N(CH_3)_2(C_2H_5)]_4$ metal source and an ozone oxidant at 250 °C on the HF-cleaned Si (100) surface. The as-grown film was amorphous and the film was crystallized as a monoclinic phase by postdeposition annealing (PDA) at 900 °C for 30 s, as was confirmed by transmission electron microscopy (TEM) and glancing angle incidence x-ray diffraction (XRD). The oxygen stoichiometry of the two films was confirmed by x-ray photoelectron spectroscopy (XPS). The Hf L_3-edge (~9.56 keV) x-ray absorptions were measured in fluorescence yield mode at room temperature at the 3C1 beamline in the Pohang Light Source (PLS). The fine structure simulation and EXAFS analyses were processed using FEFF6 code and UWXAFS package.[12]

Fine structure simulation necessitates the information on the detailed local atomic distribution near the photon-

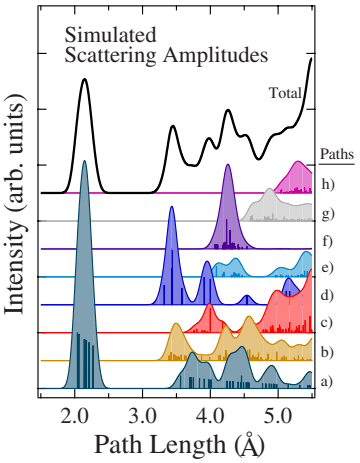

FIG. 1. (Color online) The simulated Hf L_3-edge XAFS amplitudes in the monoclinic local structure. The contribution of each path type is shown separately. The schematics of paths, (a)–(h), are exemplified in Figs. 2(a)–2(h), respectively.

absorbing atom (*ad hoc* Hf atom). Recent first-principles calculations[6,7] showed that the local coordination of Hf atoms in fully relaxed a-HfO_2 should have a range from 5 to 8. However, actual a-HfO_2 films could have many levels of the amorphousness from an ideally relaxed phase to almost polycrystalline phase, depending on the techniques and conditions adopted in the growth process. As will be shown later, the a-HfO_2 film in this study was found to have almost same Hf-O coordination number as that of the monoclinic film, implying that the knowledge of the local coordination of the a-HfO_2 film can be extended from that of the monoclinic local structure. Thus, it is reasonable that the local structure of the a-HfO_2 film is analyzed in the basis of the monoclinic local structure.

Figure 1 shows the theoretical scattering amplitudes for the *monoclinic* local structure generated by FEFF6 code.[12] Scattering amplitudes (bar typed) and broadened features of eight relevant scattering path types, labeled as (a)–(h), are shown separately. The respective path types are also depicted on the local monoclinic structure[13] in Figs. 2(a)–2(h) according to their labels. The primed atom denotes an atom other than the previous one. The effects of disorder, σ^2, and finite λ are not included in the calculation. Generally, λ is >5 Å. Hence, the exponential decay of the scattering amplitude with increasing R [see Eq. (1)] is not significant. The degree of disorder increases radically with the number of scattering events (or "legs") in the path. Therefore, the actual amplitudes of the multiple scatterings will be much lower than those shown in Fig. 1.

Nevertheless, the path $\mathrm{Hf}\rightarrow\mathrm{O}\rightarrow\mathrm{Hf}\rightarrow\mathrm{O}(\mathrm{O}')\rightarrow\mathrm{Hf}$ has a surprisingly large amplitude compared with $\mathrm{Hf}\rightarrow\mathrm{Hf}'\rightarrow\mathrm{Hf}$ or $\mathrm{Hf}\rightarrow\mathrm{O}\rightarrow\mathrm{O}'\rightarrow\mathrm{Hf}$. This path resides within the first shell, and its scattering amplitude depends on the angle between O-Hf-O bonds. Figure 3 shows the angle dependence of the relative amplitude of $\mathrm{Hf}\rightarrow\mathrm{O}\rightarrow\mathrm{Hf}\rightarrow\mathrm{O}(\mathrm{O}')\rightarrow\mathrm{Hf}$ with respect to the $\mathrm{Hf}\leftrightarrow\mathrm{O}$ single-scattering amplitude. Here the calculation was performed using a simplified cluster of a central Hf atom and two oxygen atoms in the first shell as shown in the figure. The calculated amplitudes below 50° are not reliable because of the drastically reduced muffin-tin radii of oxygen atoms. For comparison, the relative amplitudes of $\mathrm{Hf}\rightarrow\mathrm{O}\rightarrow\mathrm{O}'\rightarrow\mathrm{Hf}$ and $\mathrm{Hf}\rightarrow\mathrm{O}\rightarrow\mathrm{O}'\rightarrow\mathrm{O}\rightarrow\mathrm{Hf}$ are also appended. The actual 21 O-Hf-O angles for the monoclinic local structure[13] are shown as vertical gray lines. The total amplitude of $\mathrm{Hf}\rightarrow\mathrm{O}\rightarrow\mathrm{Hf}\rightarrow\mathrm{O}(\mathrm{O}')\rightarrow\mathrm{Hf}$ scattering should be the sum of the scattering amplitudes of 21 $\mathrm{Hf}\rightarrow\mathrm{O}\rightarrow\mathrm{Hf}\rightarrow\mathrm{O}'\rightarrow\mathrm{Hf}$ and seven $\mathrm{Hf}\rightarrow\mathrm{O}\rightarrow\mathrm{Hf}\rightarrow\mathrm{O}\rightarrow\mathrm{Hf}$. This is 1.7 and 4.3 times larger than those of $\mathrm{Hf}\rightarrow\mathrm{O}\rightarrow\mathrm{O}'\rightarrow\mathrm{Hf}$ and $\mathrm{Hf}\rightarrow\mathrm{O}\rightarrow\mathrm{O}'\rightarrow\mathrm{O}\rightarrow\mathrm{Hf}$, respectively. The total amplitudes of the respective scattering path types do not vary significantly even under the distortion of the local cluster provided the total number of nearest oxygen atoms remains at 7, as in the monoclinic structure, because most of the bond angles will lie in the region of the smooth angle variation ($50° < \theta < 150°$). Therefore, the amplitude of the multiple-scattering paths, such as the $\mathrm{Hf}\rightarrow\mathrm{O}\rightarrow\mathrm{Hf}\rightarrow\mathrm{O}(\mathrm{O}')\rightarrow\mathrm{Hf}$, can be used to indicate the intrashell structural order.

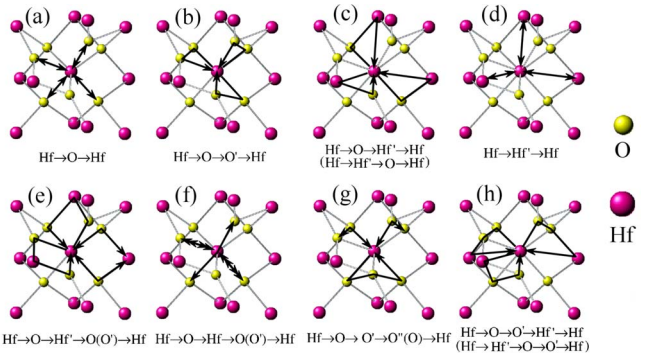

FIG. 2. (Color online) Schematic diagram of the scattering paths with the monoclinic local structure of HfO_2. (a)–(h) correspond to the respective paths (a)–(h) in Fig. 1. The prime denotes different sites from the previous one.

Figure 4 shows the experimental XANES and EXAFS spectra of the a-HfO_2 and the crystalline HfO_2 (c-HfO_2) film. The XANES features represent the transition from the deep Hf $2p_{3/2}$ core level to the unoccupied states, such as Hf $5d$ or Hf $6sp$ states. The sharp "white line" (denoted by "A") shows the relatively localized Hf $5d$ states. The line

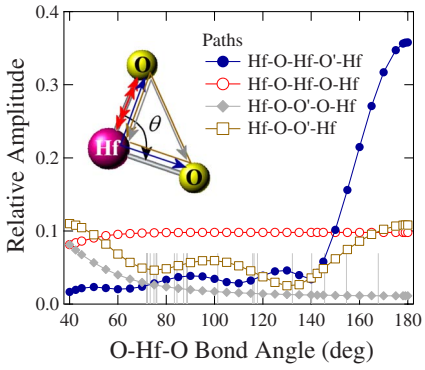

FIG. 3. (Color online) Scattering amplitudes of multiple-scattering paths in a simplified cluster composed of a central Hf atom and two equivalent oxygen atoms only. The values were normalized with respect to the amplitude of Hf-O single scattering. The vertical bars (gray) denote the angles between the O-Hf-O bonds in the first shell of monoclinic HfO_2.

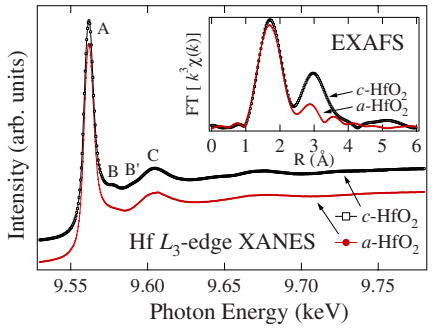

FIG. 4. (Color online) The Hf L_3-edge XANES spectra and the FT EXAFS spectra (inset) of two HfO_2 films: amorphous (a-HfO_2) and monoclinic (c-HfO_2) films. The bumps B and B′ disappear in the a-HfO_2 film.

shape and the broadness of feature A of the two spectra are almost identical. This indicates the number of d electrons of the two films to be zero; the chemistry of a-HfO_2 is same as that of c-HfO_2. The ripples (shown as B, B′, C, etc.) that appear above ~9.58 keV are the signatures of the fine structure oscillations originating from the multiple scattering of the quasi-free-final-state electrons, such as Hf 6spd states.[14] It should be noted that bumps B and B′ disappear when the film becomes amorphous. This disappearance cannot be attributed merely to peak broadening caused by increased disorder in the amorphous film[9] because the overall XANES features of the two films except for the bump have the same broadness. On the other hand, all the oscillatory behaviors can be explained by the multiple-scattering XAFS simulations, as shown in Figs. 5 and 6. The disappearance was found to be a signature of the anomalously enhanced disorder of the three path types: Hf→O→Hf→O(O′)→Hf, Hf→O→O′→Hf, and Hf→O→Hf′→Hf.

The XAFS oscillations were Fourier transformed in the k range of 2.5–9 Å^{-1}, as a function of R without correcting the phase shifts (Δ), as shown in the inset of Fig. 4. They were weighted by k^3 in order to obtain the single-scattering signatures only. The first shell of $R \sim 1.7$ Å corresponds to Hf↔O single scattering.[15–17] The first-shell intensities of the two spectra are almost identical. This indicates that the number of NNs and the disorder along the Hf-O bond direction in a-HfO_2 are similar to those in c-HfO_2 shown in Fig. 4. This suggests that the local structural order of a-HfO_2 is similar to that of monoclinic HfO_2 with seven NNs and does not include other crystal structural features, such as a tetragonal structure with eight NNs.[18]

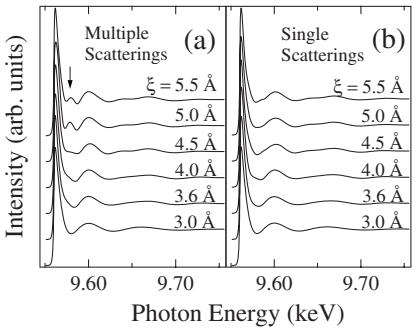

FIG. 5. The simulated Hf L_3-edge XANES spectra including (a) all multiple scattering and (b) single scattering only. The bump indicated by the arrow corresponds to bump B shown in Fig. 4.

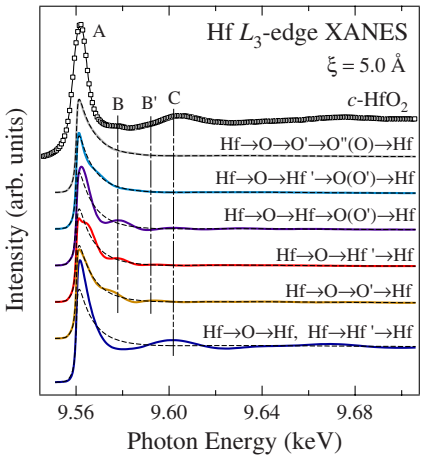

FIG. 6. (Color online) Path-type decomposition of the simulated Hf L_3-edge XANES spectra for the characteristic length ξ=5.0 Å (see the text for more details).

The second shell of R=2.5–3.3 Å is mainly due to Hf↔Hf′ single scattering, while a small portion of the magnitude is due to Hf↔O (at large displacement) single scattering and Hf→O→O→Hf multiple scattering. The decrease in the second-shell magnitude might be a signature of abridged extent of the atomistic ordering in the a-HfO_2, which is represented by a decrease in ξ. The scattering intensity of paths longer than 2ξ will be smeared out significantly due to the drastically increased disorder in the atomic positions with enhanced Debye-Waller factors.[19]

Figure 5 shows a XANES simulation that substantiates the effect of the limited characteristic length ξ in a-HfO_2. The XANES simulations were performed (a) for all multiple-scattering paths as well as (b) for the single scatterings only. The pristine x-ray absorption without the fine structure oscillation was obtained from the compilation of the x-ray absorption cross section with the McMaster correction,[20] and the fine structure oscillations calculated including scattering paths $<2\xi$ are added. Whereas there is little change in the XANES spectra for single scattering [Fig. 5(b)], the XANES line shape of multiple scattering [Fig. 5(a)] evolves with increasing ξ. A bump emerges at $\xi > 4.5$ Å in the case of multiple scattering, as denoted by the arrow in Fig. 5(a). This corresponds to bump B in the XANES spectra of c-HfO_2. The similarity between the XANES spectra of c-HfO_2 and the simulated one with high ξ and multiple scattering indicates that the multiple-scattering approach is essential for analyzing the local structure of HfO_2 films. The overall line shape of a-HfO_2 is similar to that of the simulated spectra with $\xi < 4.0$ Å only, even in the case of single scattering [Fig. 5(b)]. Therefore, the major distinction in local crystal structure of amorphous HfO_2 films from crystalline films is the decrease in the multiple-scattering factors as well as in ξ.

In order to determine the origin of the bump feature in Fig. 5, the simulated XANES spectra for ξ=5.0 Å were decomposed according to the path types, as shown in Fig. 6. The contributions of the respective path types are shown with the pristine absorption spectra (dashed lines). The ex-

TABLE I. Disorders at room temperature measured by fitting the EXAFS (Hf-O and Hf-Hf′) and XANES spectra of both monoclinic (*c*-) and amorphous (*a*-) HfO_2 films. For the EXAFS fitting, the numbers of nearest O and Hf′ scatterers (*N*) were assumed to be 7 and 11, respectively, in accordance with the monoclinic local structure (Ref. 14). The phase-corrected interatomic distances ($R+\Delta$) are also shown. The disorder in the multiple scatterings of the *a*-HfO_2 was significantly large, indicating lateral dispersion of the disorders of O atoms perpendicular to the Hf-O directions.

		c-HfO_2		*a*-HfO_2	
Fit	Paths	$R+\Delta$ (Å)	σ^2 (Å^2)	$R+\Delta$ (Å)	σ^2 (Å^2)
Hf L_3 edge	Hf-O (N=7)	2.16 ± 0.02	0.009 ± 0.002	2.14 ± 0.02	0.011 ± 0.004
EXAFS	Hf-Hf′ (N=11)	3.50 ± 0.03	0.010 ± 0.003	3.39 ± 0.03	0.021 ± 0.004
Hf L_3-edge	Hf-O-Hf-O(O′)-Hf				
XANES	Hf-O-O′-Hf		<0.03		≥0.2
	Hf-O-Hf′-Hf				

perimental XANES spectrum for *c*-HfO_2 is also shown for comparison. The bump C is originated from single scattering only, while bumps B and B′ consisted of three major multiple-scattering paths: $Hf\rightarrow O\rightarrow Hf\rightarrow O(O')\rightarrow Hf$, $Hf\rightarrow O\rightarrow O'\rightarrow Hf$, and $Hf\rightarrow O\rightarrow Hf'\rightarrow Hf$, which were observed to vanish in case of *a*-HfO_2. The contributions of the other paths were negligible.

The extinction of the multiple-scattering factors in the *a*-HfO_2 film indicates the enhanced disorder of the multiple-scattering paths [see Eq. (1)], and they can be quantified by estimating the decay rate of the XAFS oscillation in the XANES spectra as well as by using the universal mean-free path λ [see Eq. (1)]. The disorders of the single-scattering paths can also be measured quantitatively by fitting the EXAFS spectra in Fig. 4. Table I shows the fitting results for both *a*- and *c*-HfO_2 films. The multiple-scattering paths, including $Hf\rightarrow O\rightarrow Hf\rightarrow O(O')\rightarrow Hf$, $Hf\rightarrow O\rightarrow O'\rightarrow Hf$, and $Hf\rightarrow O\rightarrow Hf'\rightarrow Hf$, have a large disorder, $\sigma^2\geq0.2$ Å^2, at room temperature. This value corresponds to more than $\pm10°$ of the angular deviation in the O-Hf-O bond within the first shell. Combined with the fact that the disorder along the bond direction is only σ^2(Hf-O)~0.01 Å^2 at room temperature, this shows that the disorder in the HfO_7 cluster is highly anisotropic, i.e., the disorder in the lateral direction perpendicular to the Hf-O displacement is at least 0.1 Å^2 for each O atom.

Hence, the large disorder in the amorphous HfO_2 film occurs only in the lateral direction perpendicular to the direct Hf-O bond. This shows that the discrepancy in the dielectric properties of *a*-HfO_2 from *c*-HfO_2 is due to an increase in the number of the lateral vibronic phonons of the Hf-O bonds, not longitudinal ones. Therefore, the contribution of the lattice modulation to the dielectric properties will be significantly enhanced in *a*-HfO_2, while that of the electronic polarization via the Hf-O hybridizations is maintained as in *c*-HfO_2, which is consistent with the recent molecular-dynamics calculation results.[7] Therefore, the highly anisotropic distribution of O atoms with respect to Hf atoms is responsible for the increases in the number of Born effective charges and consequently the dielectric constant in the case of amorphous HfO_2.

The comparative XAFS study on the amorphous (*a*-) and monoclinic (*c*-) HfO_2 films revealed that the atomic order in the amorphous film is confined within 3.5 Å. Detailed path-by-path analyses further showed that the oxygen atoms have large lateral vibronic displacements, which are possibly responsible for the enhancement of dielectric constant in case of *a*-HfO_2.

This study was supported by the system IC 2010 program of the Korean government through Hynix Semiconductor Co. The experiments at the PLS were supported in part by MOST and POSTECH.

*cheolsh@snu.ac.kr

[1] G. D. Wilk, R. M. Wallace, and J. M. Anthony, J. Appl. Phys. **87**, 484 (2000).
[2] T. Yamaguchi *et al.*, Tech. Dig. - Int. Electron Devices Meet. **2001**, 451.
[3] T. J. Park *et al.*, Microelectron. Eng. **84**, 2226 (2007).
[4] J. Park *et al.*, J. Appl. Phys. **99**, 094501 (2006).
[5] X. Zhao and D. Vanderbilt, Phys. Rev. B **65**, 233106 (2002).
[6] D. Ceresoli and D. Vanderbilt, Phys. Rev. B **74**, 125108 (2006).
[7] H. Momida *et al.*, Phys. Rev. B **75**, 195105 (2007).
[8] G.-M. Rignanese, J. Phys.: Condens. Matter **17**, R357 (2005).
[9] D.-Y. Cho *et al.*, Phys. Rev. B **76**, 165411 (2007).
[10] R. Puthenkovilakam *et al.*, J. Appl. Phys. **97**, 023704 (2005).
[11] *X-Ray Absorption*, edited by D. C. Koningsberger and R. Prins (Wiley, New York, 1988).
[12] J. J. Rehr, Jpn. J. Appl. Phys., Suppl. **32-2**, 8 (1993).
[13] J. Kang, E.-C. Lee, and K. J. Chang, Phys. Rev. B **68**, 054106 (2003).
[14] J. Morais *et al.*, Appl. Phys. Lett. **86**, 212906 (2005).
[15] M. A. Sahiner *et al.*, Thin Solid Films **515**, 6548 (2007).
[16] D.-Y. Cho, S.-J. Oh, T. J. Park, and C. S. Hwang, Appl. Phys. Lett. **89**, 132904 (2006).
[17] D.-Y. Cho *et al.*, Appl. Phys. Lett. **89**, 253510 (2006).
[18] P. S. Lysaght *et al.*, Appl. Phys. Lett. **91**, 122910 (2007).
[19] J. J. Rehr and R. C. Albers, Rev. Mod. Phys. **72**, 621 (2000).
[20] *Handbook on Synchrotron Radiation*, edited by E. E. Koch (North-Holland, Amsterdam, 1983), Vol. 1.